

Determining layer number of two dimensional flakes of transition-metal dichalcogenides by the Raman intensity from substrate

Xiao-Li Li, Xiao-Fen Qiao, Wen-Peng Han, Xin Zhang,
Qing-Hai Tan, Tao Chen, Ping-Heng Tan

State Key Laboratory of Superlattices and Microstructures, Institute of Semiconductors, Chinese Academy of Sciences, Beijing 100083, China

E-mail: phtan@semi.ac.cn

Abstract. Transition-metal dichalcogenide (TMD) semiconductors have been widely studied due to their distinctive electronic and optical properties. The property of TMD flakes is a function of its thickness, or layer number (N). How to determine N of ultrathin TMDs materials is of primary importance for fundamental study and practical applications. Raman mode intensity from substrates has been used to identify N of intrinsic and defective multilayer graphenes up to $N=100$. However, such analysis is not applicable for ultrathin TMD flakes due to the lack of a unified complex refractive index (\tilde{n}) from monolayer to bulk TMDs. Here, we discuss the N identification of TMD flakes on the SiO_2/Si substrate by the intensity ratio between the Si peak from 100-nm (or 89-nm) SiO_2/Si substrates underneath TMD flakes and that from bare SiO_2/Si substrates. We assume the real part of \tilde{n} of TMD flakes as that of monolayer TMD and treat the imaginary part of \tilde{n} as a fitting parameter to fit the experimental intensity ratio. An empirical \tilde{n} , namely, \tilde{n}_{eff} , of ultrathin MoS_2 , WS_2 and WSe_2 flakes from monolayer to multilayer is obtained for typical laser excitations (2.54 eV, 2.34 eV, or 2.09 eV). The fitted \tilde{n}_{eff} of MoS_2 has been used to identify N of MoS_2 flakes deposited on 302-nm SiO_2/Si substrate, which agrees well with that determined from their shear and layer-breathing modes. This technique by measuring Raman intensity from the substrate can be extended to identify N of ultrathin 2D flakes with N -dependent \tilde{n} . For the application purpose, the intensity ratio excited by specific laser excitations has been provided for MoS_2 , WS_2 and WSe_2 flakes and multilayer graphene flakes deposited on Si substrates covered by 80-110 nm or 280-310 nm SiO_2 layer.

1. Introduction

With the advent of graphene and the exfoliation technique for preparing atomically thin sheets,[1] layered materials(LMs) sparked wide interest in the world.[2] Among the LMs, transition-metal dichalcogenide(TMD) $2H-MX_2$ ($M=Mo, W; X=S, Se$) semiconductors have been widely studied due to their distinctive electronic and optical properties.[3, 4, 5] They have an X-M-X covalently bonded sandwich structure in each layer, and the layers are weakly stacked by van der Waals force. Such stacked layer structure makes it possible to peel off different layers from bulk. The property of TMD flakes is a function of its thickness, or layer number (denoted as N).[3, 6, 7, 8, 9, 10]. For example, the band gap of MoS_2 , WS_2 and WSe_2 exhibits an indirect-to-direct transition from a few-layer to monolayer thickness,[3, 6] enabling many applications in electronics and optoelectronics. Thus, how to determine N of ultrathin TMDs materials is of primary importance for fundamental study and practical applications.

Several optical techniques have been developed to identify N of the TMD flakes, such as photoluminescence (PL) and optical contrast.[5] PL can be used to distinguish 1L from multilayer (ML) because of its strong and narrow PL peak.[3] Optical contrast is not sensitive to the flake quality and the stacking structure of 2D flakes,[11, 12, 13] and thus it has been widely used to identify N of graphene flakes by comparing the experimental value with the theoretical one for different N thanks to almost identical complex refractive index (\tilde{n}) from 1L graphene (1LG) to ML graphene (MLG).[13, 14] However, quantitative analysis of optical contrast of ultrathin TMD flakes on SiO_2/Si substrate is difficult because there exist abundant features associated with optical transitions in the wavelength (λ) dependent \tilde{n} for TMD flakes and \tilde{n} of TMD flakes itself significantly depends on N due to the indirect-to-direct transition from ML to 1L.[15, 16]

The ultra-low Raman spectroscopy has been used to reliably determine N for MLG, TMD flakes and 2D alloy flakes.[17, 8, 18] However, this technique requires expensive adapters and nonstandard equipment setup. Therefore, it is essential to look for the technique for N identification only by the standard Raman system. Recently, Raman mode intensity from substrates has been used to identify N of intrinsic and defective MLGs up to $N=100$. [19] This technique is difficult to be applied to the TMD flakes due to the lack of unified \tilde{n} for TMD flakes from 1L to ML. However, the calculation of Raman mode intensity from substrates only requires \tilde{n} at the wavelengths of the laser excitation and the scattered photon, and thus, in this letter, we try to extend this technique for N determination of TMD flakes deposited onto the SiO_2/Si substrate. By fitting the experimental data of the intensity ratio between the Si peak from SiO_2/Si substrates underneath TMD flakes and that from bare SiO_2/Si substrates, we obtained empirical \tilde{n} , namely, \tilde{n}_{eff} , for ultrathin MoS_2 , WS_2 and WSe_2 flakes at different laser excitation wavelengths. The fitted \tilde{n}_{eff} of MoS_2 has been used to determine N of MoS_2 flakes on Si substrate covered by 302 nm SiO_2 , which agrees well with that determined from their shear and layer-breathing modes[8].

2. Experimental details

Ultra-thin MoS₂, WS₂ and WSe₂ flakes were mechanically exfoliated from bulk MoS₂, WS₂ and WSe₂ (purchased from 2d Semiconductors, Inc.), and transferred onto Si substrates covered with SiO₂ film with different thickness (h_{SiO_2} , 100 nm, 89 nm, or 302 nm). Raman measurements were performed at room temperature using a Jobin-Yvon HR800 micro-Raman system equipped with a liquid nitrogen-cooled charge couple detector (CCD), a $\times 50$ objective lens with a numerical aperture (N.A.) of ~ 0.45 and a 1800 lines/mm grating. The excitation energies (ε_L) are 2.09 eV from a He-Ne laser, 2.34 eV and 2.54 eV from a Kr⁺ laser. Plasma lines were removed from the laser beam by BragGrate Bandpass filters. Measurements down to 5 cm⁻¹ are enabled by three BragGrate notch filters with optical density 3 and with full width at half maximum (FWHM) of 8 cm⁻¹. [8] Both BragGrate bandpass and notch filters are produced by OptiGrate Corp. The typical laser power is about 0.4 mW to avoid sample heating.

3. Results and discussion

3.1. \tilde{n}_{eff} of MoS₂ flakes fitted from N -dependent Si mode intensity

We denote a N -layer TMD flake as NL-TMD, such as NL-MoS₂, NL-WS₂ and NL-WSe₂, and thus monolayer MoS₂ is denoted as 1L-MoS₂. 1-10L MoS₂ flakes were pre-estimated by the Raman measurements of the ultralow-frequency shear (C) and layer-breathing (LB) modes, as previously done for MoS₂ and MoWS₂ flakes. [8, 18] Fig.1(a) shows the high-frequency Raman spectra of 1L-10L MoS₂ along with Si mode from substrate were measured by ε_L of 2.34 eV. Because of the different symmetry between even and odd NL-TMDs and bulk TMDs, the corresponding two Raman-active modes E_{2g}^1 and A_{1g} in bulk TMDs should be assigned as the E' and A'_1 in odd NL-TMDs and the E_g and A_{1g} modes in even NL-TMDs, [5, 20] respectively. However, to see the evolution from 1L to NL ($N > 1$), hereafter the two modes for all cases are simply labeled as E_{2g}^1 and A_{1g} , as commonly done in the literature. [5, 7, 21] With increasing N , the peak position difference between the E_{2g}^1 and A_{1g} modes, $\Delta\omega(A - E) = \text{Pos}(A_{1g}) - \text{Pos}(E_{2g}^1)$, increases from 17.4 cm⁻¹ for 1L to 25 cm⁻¹ for 10L, following the formula of $\Delta\omega(A - E) = 25.8 - 8.4/N$. [5] The peak area of the E_{2g}^1 and A_{1g} modes, $I(E_{2g}^1)$ and $I(A_{1g})$, increases with N up to $N=4$ and then gradually decreases with N , as shown in Fig.1(b), after normalized by the peak area of the Si mode ($I_0(\text{Si})$) from bare substrate that is not covered by MoS₂ flakes. Obviously, $I(E_{2g}^1)/I_0(\text{Si})$ and $I(A_{1g})/I_0(\text{Si})$ can not be used to identify N for few-layer MoS₂.

Fig.1(a) shows that peak area of the Si mode, $I_{2D}(\text{Si})$, from the substrate underneath MoS₂ flakes monotonously decreases with increasing N . Now we focus on $I_{2D}(\text{Si})$ itself. To exclude the effect of crystal orientation on the Raman intensity, $I_{2D}(\text{Si})$ is normalized by $I_0(\text{Si})$. The maximum of $I_0(\text{Si})$ can be obtained by rotating the Si wafer and adjusting the focus of laser beam onto the Si substrate, then, we directly moved the laser spot to MoS₂ flake to measure $I_{2D}(\text{Si})$ to ensure a good signal-to-noise ratio of $I_{2D}(\text{Si})/I_0(\text{Si})$.

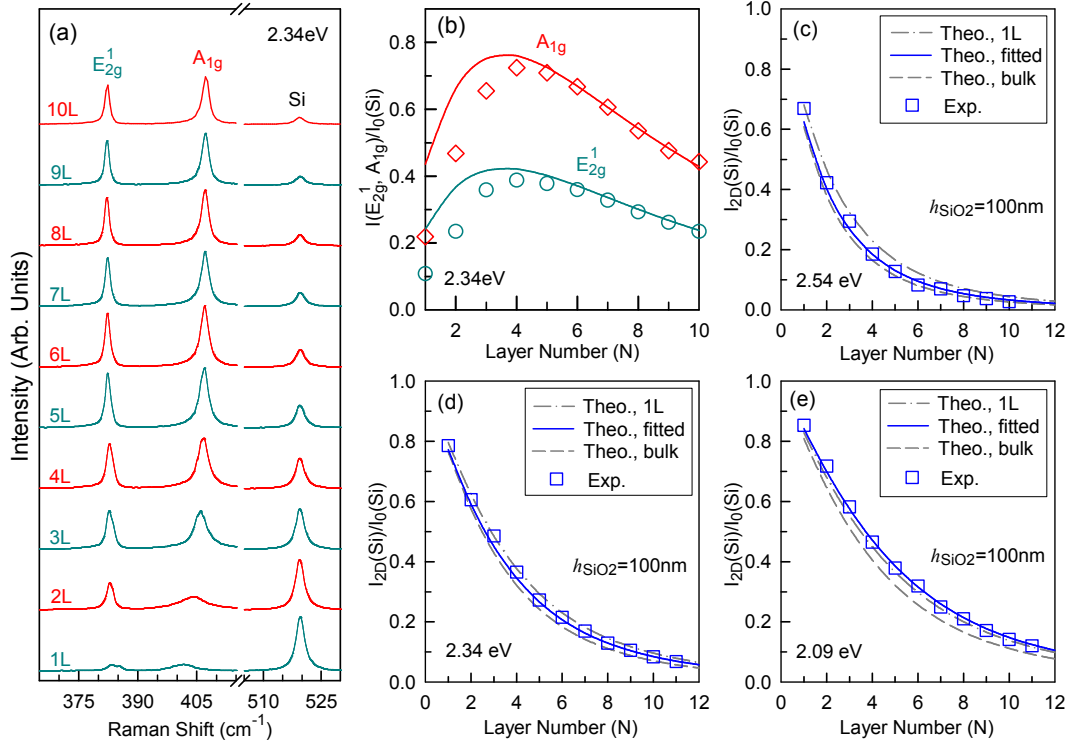


Figure 1. (a) Raman spectra of NL-MoS₂ with N from 1 to 10 in the range of the E_{2g}¹, A_{1g} and Si modes for $\varepsilon_L=2.34$ eV, where N is determined by the C and LB modes of the flakes. (b) N-dependent $I(E_{2g}^1)/I_0(\text{Si})$ and $I(A_{1g})/I_0(\text{Si})$ and the corresponding theoretical curves calculated from \tilde{n}_{eff} . The experimental (Exp., squares) and theoretical (Theo., solid, dashed, and dash-dotted lines) data of $I_{2D}(\text{Si})/I_0(\text{Si})$ related with NL-MoS₂ flakes as a function of N for the excitation energies of (c) 2.54 eV, (d) 2.34 eV and (e) 2.09 eV. $h_{\text{SiO}_2} = 100$ nm. The dashed, dash-dotted and solid lines are calculated based on the \tilde{n} for 1L-MoS₂ and bulk-MoS₂ and the fitted \tilde{n}_{eff} for NL-MoS₂, respectively.

Figs.1(c-e) depicts the N-dependent $I_{2D}(\text{Si})/I_0(\text{Si})$ (squares) for NL-MoS₂ flakes on SiO₂/Si substrate ($h_{\text{SiO}_2} = 100$ nm) excited by ε_L of 2.54 eV, 2.34 eV and 2.09 eV, clearly showing the monotonous decrease in intensity with increasing N. The laser beam to Si substrate is initially adsorbed by the MoS₂ flake and the Raman signal from Si substrate is adsorbed again by the MoS₂ flake, similar to the case of MLGs.[19]. This make $I_{2D}(\text{Si})/I_0(\text{Si})$ sensitive to N of MoS₂ flakes, implying its possibility of N identification for MoS₂ flakes.

$I_{2D}(\text{Si})$ can be calculated by using multiple reflection interference method and transfer matrix formalism for multilayered structures[19], which can be expressed in air/NL-MoS₂/SiO₂/Si four-layer structure as the following equation:

$$I_{2D}(\text{Si}) \propto \int_0^{h_{\text{SiO}_2}} \int_0^{\arcsin(N.A.)} \int_0^{2\pi} \int_0^{\arcsin(N.A.)} \int_0^{2\pi} \sum_{i=s,p_{\perp},p_{\parallel}} \sum_{j=s',p'_{\perp},p'_{\parallel}} \left| F_L^i(z, \theta, \varphi) F_R^j(z, \theta', \varphi') \right|^2 \sin \theta \cos \theta d\theta d\varphi \sin \theta' \cos \theta' d\theta' d\varphi' dz, \quad (1)$$

where the Raman intensity is given by integrating over the solid angle ($\arcsin(N.A.)$) of microscope objective (θ, φ for the laser beam and θ', φ' for the Raman signal) and the

penetration depth of laser excitation into Si layer ($h_{Si} \approx 2\mu m$). Different from the case of normal incidence where $\theta, \varphi, \theta', \varphi' = 0$, the s-polarization (transverse electric field, \vec{E} , perpendicular to the NL-MoS₂ c-axis) and the p-polarization (transverse magnetic field, \vec{H} , associated to electric field by $\vec{H} = \tilde{n}\vec{E}$) field components are considered separately for the oblique incidence, which are involved in the laser excitation enhancement factor F_L and Raman scattering enhancement factor F_R . F_L and F_R are calculated by using transfer matrix formalism, in which complex refractive index (\tilde{n}) and thickness (h) of each medium should be known in advance. $I_0(\text{Si})$ can be obtained by setting the thickness of MoS₂ flakes to be zero. The detailed derivation process can be obtained in supplementary data.

$I_{2D}(\text{Si})/I_0(\text{Si})$ is expected to be sensitive to N, N.A. of the objective used, ε_L and h_{SiO_2} , as demonstrated in the case of MLGs.[19] A variation of 10 nm for h_{SiO_2} can introduce a change on the N-dependent $I_{2D}(\text{Si})/I_0(\text{Si})$,[19] therefore, a precise determination of h_{SiO_2} is very important for N identification of NL-MoS₂ flakes on SiO₂/Si substrates by $I_{2D}(\text{Si})/I_0(\text{Si})$. As a simple, fast and nondestructive technique, optical contrast measurement can be used to determine h_{SiO_2} with a typical micro-Raman confocal system.[14] It is found that an effective N.A. must be used to calculate optical contrast of multilayer graphene deposited on SiO₂/Si substrates once the commonly-used 100× objective with N.A. of ~ 0.9 is used for optical microscope.[12, 13, 19] In this work, the 50× objective with N.A. of 0.45 is used to measure $I_{2D}(\text{Si})/I_0(\text{Si})$. In fact, as shown in the Supplementary Data, it is found that $I_{2D}(\text{Si})/I_0(\text{Si})$ is not sensitive to N.A. when $\text{N.A.} \leq 0.5$ and $N \leq 10$ for NL-MoS₂ flakes on SiO₂/Si substrates.

The unified $\tilde{n} = n - i\kappa$ for MoS₂ flakes from 1L to ML is necessary to calculate N-dependent $I_{2D}(\text{Si})/I_0(\text{Si})$, where n and κ are the real and imaginary parts of \tilde{n} , respectively. However, both n and κ for MoS₂ flakes are found to be sensitive to N in the visible region.[15, 16] λ -dependent \tilde{n} of 1L-MoS₂ and bulk MoS₂ are obtained according to their complex dielectric functions[15] using a formula of $\tilde{n}^2 = \tilde{\varepsilon}$. If we apply \tilde{n} of 1L-MoS₂ or bulk MoS₂ to all the NL-MoS₂ flakes, $I_{2D}(\text{Si})/I_0(\text{Si})$ can be calculated for the three ε_L , as shown in Figs.1(c-e) by dash-dotted and dashed lines, respectively. Both of them do not fit well to the experimental data. When $\varepsilon_L = 2.54$ eV and 2.34 eV, the experimental data lay in between the two theoretical curves. However, when $\varepsilon_L = 2.09$ eV excitation, the experimental data are larger than the two theoretical ones because it is under the near-resonant condition with the B exciton.[3, 10]

In order to identify N by $I_{2D}(\text{Si})/I_0(\text{Si})$, an empirical \tilde{n} , namely, \tilde{n}_{eff} , is necessary to be adopted for MoS₂ flakes to minimize the difference between the theoretical and experimental data. If we do not consider the multiple reflection interference effect, the difference between $I_{2D}(\text{Si})$ and $I_0(\text{Si})$ results from the adsorption of the laser beam and Raman beam when they pass through the MoS₂ flakes, which is mainly dominated by the imaginary part (κ) of \tilde{n} of MoS₂, but not by the real part (n) of \tilde{n} of MoS₂. Thus, we assume the real part of \tilde{n}_{eff} , namely, n_{eff} , of MoS₂ flakes as n of 1L-MoS₂. Also, as an approximation, we neglect the difference of \tilde{n}_{eff} between the wavelengths of laser

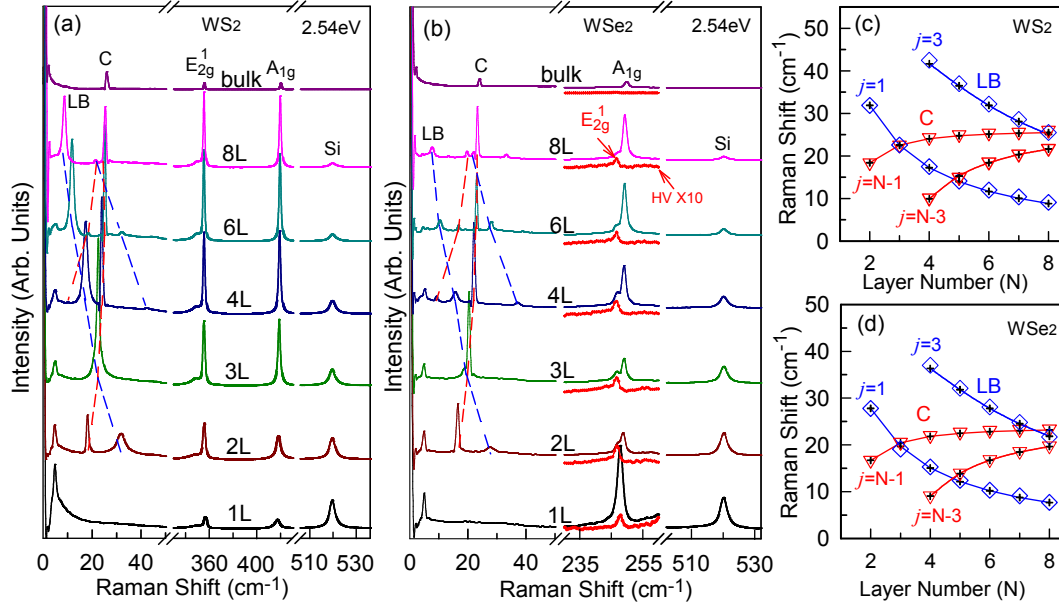


Figure 2. Raman spectra of (a) NL-WS₂ and (b) NL-WSe₂ in the ultra-low frequency range and in the range of the E_{2g}¹, A_{1g} and Si modes for $\varepsilon_L=2.54$ eV. Pos(C) and Pos(LB) in (c) NL-WS₂ and (d) NL-WSe₂ as a function of N. $j=1,3$ and $j=N-1$ and $N-3$ correspond to the observed branches of the Sin diagram, see text.

excitation and Raman beam. Finally, we can obtain the imaginary part of \tilde{n}_{eff} , namely, κ_{eff} , of MoS₂ flakes by fitting the experimental $I_{2D}(\text{Si})/I_0(\text{Si})$ by the theoretical ones for each excitation wavelength. We found that, indeed, a κ_{eff} can make the theoretical $I_{2D}(\text{Si})/I_0(\text{Si})$ agree well with the experimental ones, as shown in Figs.1(c-e) by solid curves. The fitted κ_{eff} along with n_{eff} for MoS₂ flakes are summarized in Table 1 for ε_L of 2.54 eV, 2.34 eV and 2.09 eV. In this case, we can calculate $I_{2D}(\text{Si})/I_0(\text{Si})$ based on the fitted \tilde{n}_{eff} for MoS₂ flakes and compare them with the experimental one, N of MoS₂ flakes can be determined. Based on the fitted \tilde{n}_{eff} for MoS₂ flakes, we calculated $I(E_{2g}^1)/I_0(\text{Si})$ and $I(A_{1g})/I_0(\text{Si})$ as a function of N for $\varepsilon_L=2.34$ eV, where adjustable parameters were introduced to take different efficiencies among E_{2g}¹, A_{1g} and Si modes into account. The results are shown by solid curves in Fig.1(b). The theoretical results basically correspond with the experimental ones, but there exists significant discrepancy for $N < 5$.

3.2. \tilde{n}_{eff} of NL-WS₂ and NL-WSe₂ flakes

Now we check the possibility to apply this technique to other TMDs, such as WS₂ and WSe₂. We obtain 1-8L WS₂ and WSe₂ flakes by mechanical exfoliation from bulk crystal and N is determined by the C and LB modes based on the method described in Ref.[18]. The C and LB modes and the E_{2g}¹ and A_{1g} modes of 1-8L WS₂ and WSe₂ were measured by 2.54-eV laser excitation at room temperature, as depicted in Figs.2(a) and 2(b), respectively. Pos(C) and Pos(LB) of 2-8L WS₂ and WSe₂ are summarized in Figs.2(c) and 2(d), respectively. Besides a fan diagram[8], the N-dependent Pos(C) and

Pos(LB) can also exhibit a Sin diagram[22], which can be written as follows:

$$\begin{aligned}\omega(C_{N,N-j}) &= \sqrt{2}\omega(C_{21})\sin(\frac{j\pi}{2N}), \\ \omega(LB_{N,N-j}) &= \sqrt{2}\omega(LB_{21})\sin(\frac{j\pi}{2N}).\end{aligned}\tag{2}$$

where j is an integer, $j=N-1, N-2, \dots, 2, 1$. $\omega(C_{21})$ and $\omega(LB_{21})$ are the frequencies of the C and LB modes in 2L flakes, respectively. The measured C modes in bulk WS₂ and WSe₂ are located at 26.3 and 23.9 cm⁻¹, and then the measured $\omega(C_{21})$ ($\omega(LB_{21})$) of 2L-WS₂ and 2L-WSe₂ are 18.4 (31.9) and 16.7 (27.8) cm⁻¹, respectively. Each branch in Eq. (1) always decreases or increases in frequency with increasing N. As indicted by the solid lines in Figs.2(c) and 2(d), the branches of $j = N - 1$ and $j = N - 3$ are observed for the C modes, and the branches of $j = 1$ and $j = 3$ are observed for the LB modes.

The E_{2g}¹ and A_{1g} modes of 1-8L WS₂ and WSe₂ are found to be insensitive to N, as addressed in previous works[9, 23]. The E_{2g}¹ mode of WSe₂ flakes is very weak and it can be clearly revealed under cross (HV) polarization configuration, as shown in Fig.2(b). The frequency shift of both E_{2g}¹ and A_{1g} modes for NL-WS₂ and NL-WSe₂ is less than 3 cm⁻¹, which make it difficult for N determination.

I_{2D}(Si) from Si substrate underneath WS₂ and WSe₂ flakes decreases with increasing N, as shown in Figs.2(a) and 2(b), similar to the case of MoS₂ flakes in Fig.1(a). This suggests that I_{2D}(Si)/I₀(Si) can be used for N identification of WS₂ and WSe₂ flakes deposited on SiO₂/Si substrate. I_{2D}(Si)/I₀(Si) for NL-WS₂ and NL-WSe₂ flakes as a function of N (N=1,2,...,8) for $h_{SiO_2} = 89$ nm were measured for two excitations: $\varepsilon_L=2.54$ eV and 2.34 eV. Indeed, I_{2D}(Si)/I₀(Si) monotonously decreases with increasing N for WS₂ and WSe₂ flakes excited by the two excitations. The corresponding experimental data were depicted in Fig.3 by triangles and circles, respectively. Considering that the 2.09-eV excitation is almost resonant with the A exciton of 1L-WS₂ and B exciton of 1L-WSe₂,[24], the 2.09-eV laser excitation is not used for WS₂ and WSe₂ flakes.

To understand the N-dependent I_{2D}(Si)/I₀(Si) of WS₂ and WSe₂ flakes for their N determination, similar to the case of MoS₂ flakes as discussed above, we assume n_{eff} of WS₂ and WSe₂ flakes as n of 1L-WS₂ and 1L-WSe₂[15], respectively. κ_{eff} of WS₂ and WSe₂ flakes have been used as a fitting parameter to fit the experimental I_{2D}(Si)/I₀(Si). The \tilde{n}_{eff} of WS₂ and WSe₂ flakes for $\varepsilon_L=2.54$ and 2.34 eV are summarized in Table 1. The calculated I_{2D}(Si)/I₀(Si) based on the fitted \tilde{n}_{eff} are shown by solid lines in Fig.3, which agree well with the experimental values.

3.3. Identifying Layer number of MoS₂ flakes deposited on 302-nm SiO₂/Si substrate

As discussed above, the empirical \tilde{n}_{eff} of MoS₂, WS₂ and WSe₂ flakes are obtained by fitting the theoretical I_{2D}(Si)/I₀(Si) to the experimental data excited by different excitation energies. Once \tilde{n}_{eff} for TMD flakes at specific ε_L is available, one can compare the theoretical I_{2D}(Si)/I₀(Si) with the corresponding experimental data excited by the same ε_L to determine N of the TMD flakes. As an example, we apply this technique to

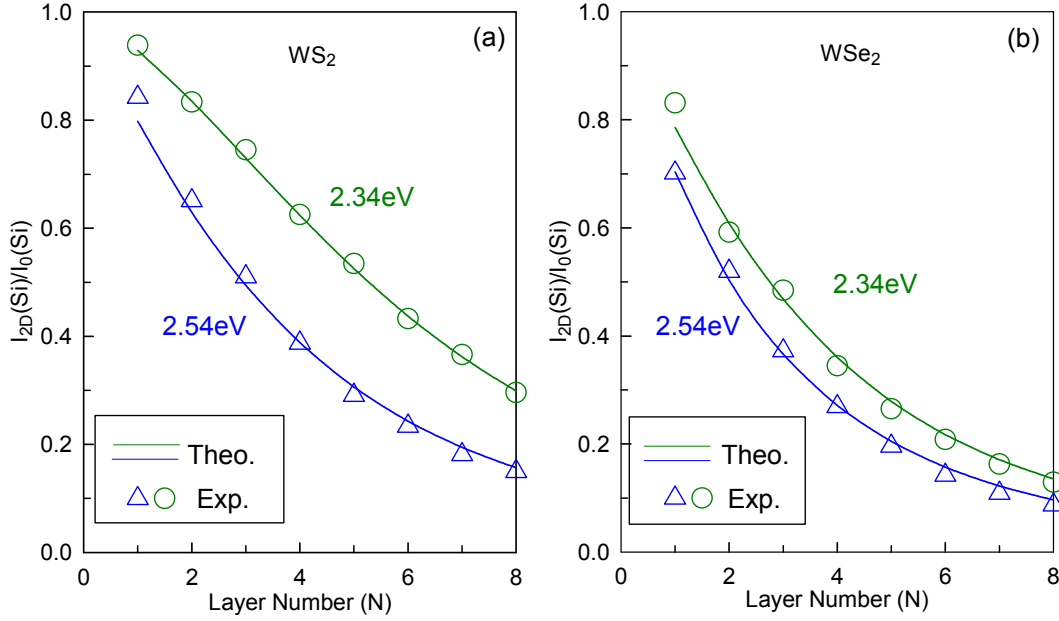


Figure 3. The experimental (Exp., triangles and circles) and theoretical (Theo., solid lines) data of $I_{2D}(Si)/I_0(Si)$ for the excitation energies of $\varepsilon_L=2.54$ eV and 2.34 eV as a function of N . (a) NL-WS₂, (b) NL-WSe₂. $h_{SiO_2} = 89$ nm.

Table 1. The empirical \tilde{n}_{eff} ($n_{eff}-i\kappa_{eff}$) of MoS₂, WS₂ and WSe₂ flakes to calculate $I_{2D}(Si)/I_0(Si)$ at different ε_L .

	MoS ₂	WS ₂	WSe ₂
ε_L (eV)	2.54 2.34 2.09	2.54 2.34	2.54 2.34
n_{eff}	5.29 4.85 4.58	4.40 4.62	4.22 4.64
κ_{eff}	1.85 1.20 1.22	1.10 0.48	1.86 1.40

MoS₂ flakes on Si substrate covered by 302-nm SiO₂ film, where N is precisely determined by the C and LB modes of MoS₂ flakes[8] and $N = 1, 3, 4, 6, 7$. Based on the fitted \tilde{n}_{eff} for MoS₂ flakes, the theoretical $I_{2D}(Si)/I_0(Si)$ were calculated as a function of N for $\varepsilon_L=2.09, 2.34$ and 2.54 eV, as shown by crosses and solid lines in Figs.4(a-c), respectively. They agree well with the experimental data, as depicted by squares in Fig.4. The N -dependent $I_{2D}(Si)/I_0(Si)$ of TMD flakes is found to be sensitive to ε_L , as demonstrated in Figs.1 and 3. Thus, the determined N of TMD flakes by an excitation energy can be confirmed from further measurement by another excitation energy, which leads to an accurate N determination of ultrathin TMD flakes by the Raman intensity from substrate.

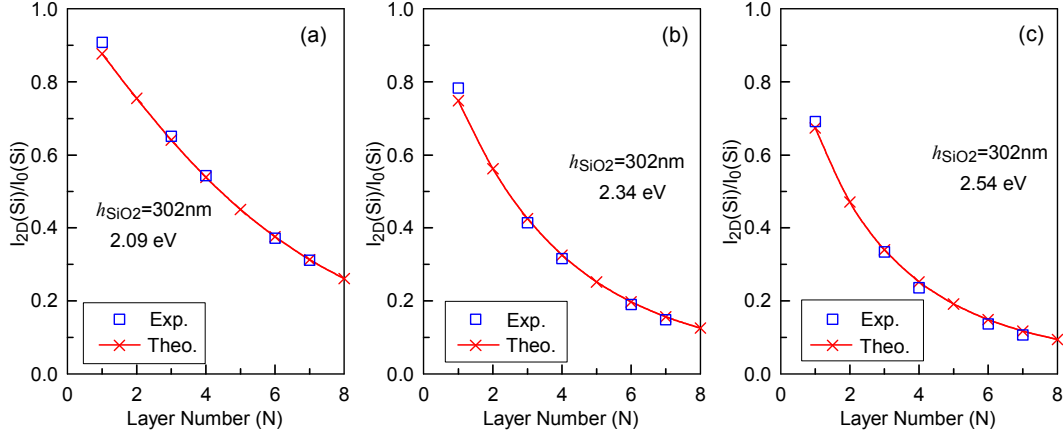


Figure 4. The experimental (Exp., squares) and theoretical (Theo., solid lines and crosses) data of $I_{2D}(Si)/I_0(Si)$ related with NL-MoS₂ flakes as a function of N for the excitation energies of (a) 2.09 eV, (b) 2.34 eV and (c) 2.54 eV. The solid lines are calculated based on the fitted \tilde{n}_{eff} from Figure 2. $h_{SiO_2} = 302$ nm.

4. Conclusions

In conclusion, a technique to determine N of TMD flakes such as MoS₂, WS₂ and WSe₂ deposited on SiO₂/Si substrate has been proposed by measuring $I_{2D}(Si)/I_0(Si)$, i.e., the intensity ratio of the Si peak from SiO₂/Si substrates underneath the 2D flakes of TMDs to that from bare SiO₂/Si substrates. The real part of the empirical \tilde{n}_{eff} of TMD flakes is assumed as that of 1L TMD. The κ_{eff} is a fitting parameter to the experimental intensity ratio between the Si peak from SiO₂/Si substrates underneath TMD flakes and that from bare SiO₂/Si substrates. The empirical \tilde{n}_{eff} of MoS₂, WS₂ and WSe₂ flakes for ϵ_L of 2.54, 2.34 or 2.09 eV is obtained. The resulted \tilde{n}_{eff} of MoS₂ flakes has been used to identify N of MoS₂ flakes deposited on 302-nm SiO₂/Si substrate. This opens the possibility to identify N of ultrathin 2D flakes with N -dependent complex refractive index by measuring Raman intensity from the substrate. For the sake of N identification of TMD and MLG flakes for research community, $I_{2D}(Si)/I_0(Si)$ of TMD flakes deposited on SiO₂/Si substrate is enclosed in the supplementary data for commonly-used excitation energies (2.34 eV and 2.54 eV) and SiO₂ thickness (80-110nm and 280-310nm), along with the corresponding data for MLG.

5. Acknowledgments

We acknowledge support from the National Natural Science Foundation of China, grants 11225421, 11434010, 11474277 and 11504077.

6. References

- [1] Novoselov K S, Geim A K, Morozov S V, Jiang D, Zhang Y, Dubonos S V, Grigorieva I V and Firsov A A 2004 *Science* **306** 666

- [2] Chhowalla M, Shin H S, Eda G, Li L J, Loh K P and Zhang H 2013 *Nat. Chem.* **5** 263
- [3] Mak K F, Lee C, Hone J, Shan J and Heinz T F 2010 *Phys. Rev. Lett.* **105** 136805
- [4] Wang Q H, Kalantar-Zadeh K, Kis A, Coleman J N and Strano M S 2012 *Nat. Nanotechnol.* **7** 699
- [5] Zhang X, Qiao X F, Shi W, Wu J B, Jiang D S and Tan P H 2015 *Chem. Soc. Rev.* **44** 2757
- [6] Splendiani A, Sun L, Zhang Y B, Li T S, Kim J, Chim C Y, Galli G and Wang F 2010 *Nano Lett.* **10** 1271
- [7] Lee C, Yan H, Brus L E, Heinz T F, Hone J and Ryu S 2010 *ACS Nano* **4** 2695
- [8] Zhang X, Han W P, Wu J B, Milana S, Lu Y, Li Q Q, Ferrari A C and Tan P H 2013 *Phys. Rev. B* **87** 115413
- [9] Terrones H, Del Corro E, Feng S, Poumirol J M, Rhodes D, Smirnov D, Pradhan N R, Lin Z, Nguyen M A T, Elias A L, Mallouk T E, Balicas L, Pimenta M A and Terrones M 2014 *Sci. Rep.* **4** 4215
- [10] Lee J U, Park J, Son Y W and Cheong H 2015 *Nanoscale* **7** 3229
- [11] Ni Z H, Wang H M, Kasim J, Fan H M, Yu T, Wu Y H, Feng Y P and Shen Z X 2007 *Nano Lett.* **7** 2758
- [12] Casiraghi C, Hartschuh A, Lidorikis E, Qian H, Harutyunyan H, Gokus T, Novoselov K S and Ferrari A C 2007 *Nano Lett.* **7** 2711
- [13] Han W P, Shi Y M, Li X L, Luo S Q, Lu Y and Tan P H 2013 *Acta Phys. Sin.* **62** 110702
- [14] Lu Y, Li X L, Zhang X, Wu J B and Tan P H 2015 *Sci. Bull.* **60** 806
- [15] Li Y L, Chernikov A, Zhang X, Rigosi A, Hill H M, van der Zande A M, Chenet D A, Shih E M, Hone J and Heinz T F 2014 *Phys. Rev. B* **90** 205422
- [16] Park J W, So H S, Kim S, Choi S H, Lee H, Lee J, Lee C and Kim Y 2014 *J. Appl. Phys.* **116** 183509
- [17] Tan P H, Han W, Zhao W, Wu Z, Chang K, Wang H, Wang Y, Bonini N, Marzari N and Pugno N o 2012 *Nat. Mater.* **11** 294–300
- [18] Qiao X F, Li X L, Zhang X, Shi W, Wu J B, Chen T and Tan P H 2015 *Appl. Phys. Lett.* **106** 223102
- [19] Li X L, Qiao X F, Han W P, Lu Y, Tan Q H, Liu X L and Tan P H 2015 *Nanoscale* **7** 8135
- [20] Molina-Sanchez A and Wirtz L 2011 *Phys. Rev. B* **84** 155413
- [21] Li S L, Miyazaki H, Song H, Kuramochi H, Nakaharai S and Tsukagoshi K 2012 *ACS Nano* **6** 7381
- [22] Wu J B, Hu Z X, Zhang X, Han W P, Lu Y, Shi W, Qiao X F, Ijias M, Milana S, Ji W, Ferrari A C and Tan P H 2015 *ACS Nano* **9** 7440
- [23] Zhao W J, Ghorannevis Z, Amara K K, Pang J R, Toh M, Zhang X, Kloc C, Tan P H and Eda G 2013 *Nanoscale* **5** 9677
- [24] Zhao W J, Ghorannevis Z, Chu L Q, Toh M L, Kloc C, Tan P H and Eda G 2013 *Acs Nano* **7** 791

Supplementary Data

Determining layer number of two dimensional flakes of multilayer graphenes and transition-metal dichalcogenides by the Raman intensity from substrate

Xiao-Li Li¹, Xiao-Fen Qiao¹, Wen-Peng Han¹, Xin Zhang¹, Qing-Hai Tan¹, Tao Chen¹, and Ping-Heng Tan¹

1.State Key Laboratory for Superlattices and Microstructures, Institute of Semiconductors, Chinese Academy of Sciences, Beijing 100083, China E-mail: phtan@semi.ac.cn

Content

1. Calculating the Si mode intensity from SiO₂/Si substrates underneath TMD flakes ($I_{2D}(\text{Si})$) and that ($I_0(\text{Si})$) from bare SiO₂/Si substrates.
2. $I_{2D}(\text{Si})/I_0(\text{Si})$ for NL-TMDs deposited on SiO₂/Si substrate.
3. $I_{2D}(\text{Si})/I_0(\text{Si})$ for N Layer graphenes deposited on SiO₂/Si substrate.

1. Calculating the Si mode intensity from SiO₂/Si substrates underneath TMD flakes ($I_{2D}(\text{Si})$) and that ($I_0(\text{Si})$) from bare SiO₂/Si substrates

Raman intensity in multilayer structure is determined by multiple reflection at the interfaces and optical interference within the medium. We adopt the multiple reflection interference method^[1–4,8] to calculate the Raman mode intensity of a medium in the multilayer structure. When N layer (NL) transition-metal dichalcogenide (TMD) flakes (NL-MX₂) are deposited on SiO₂/Si substrate, the four-layer structure can be established, containing air(\tilde{n}_0), NL(\tilde{n}_1, d_1), SiO₂(\tilde{n}_2, d_2), Si(\tilde{n}_3, d_3), where \tilde{n}_i and d_i ($i=0,1,2,3$) are the complex refractive index and the thickness of each medium, respectively, as demonstrated in Fig. S1.

In the following text, we will discuss how to calculate the Si mode intensity from SiO₂/Si substrates underneath TMD flakes ($I_{2D}(\text{Si})$) and that ($I_0(\text{Si})$) from bare SiO₂/Si substrates.

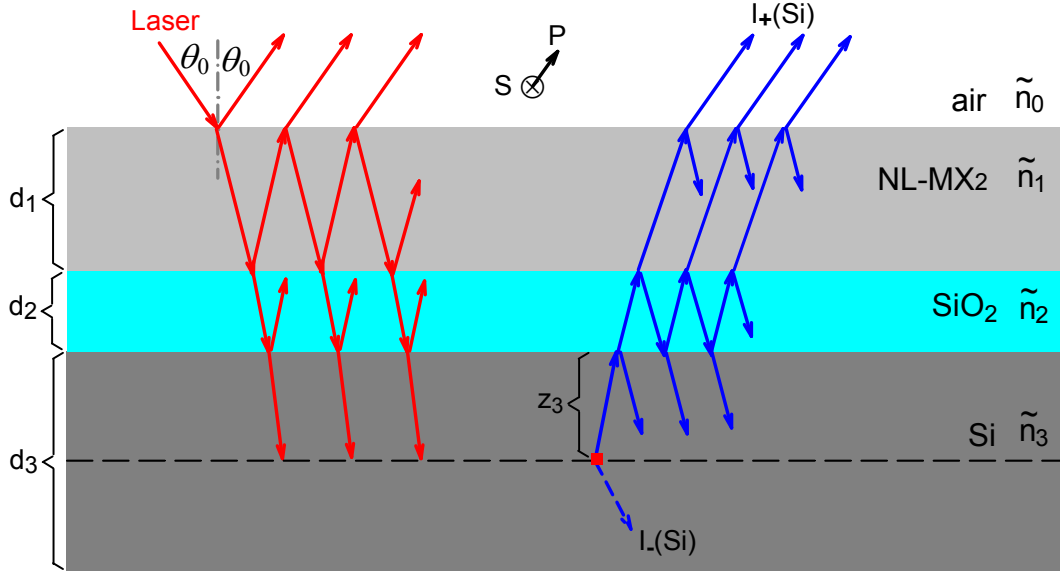


Figure 1 Schematic diagrams of multiple reflection and optical interference in the multilayer structures containing air, NL-MX₂, SiO₂, and Si for the incident laser and out-going Raman signals of the Si peak from Si substrate. \tilde{n}_0 , \tilde{n}_1 (d_1), \tilde{n}_2 (d_2), and \tilde{n}_3 (d_3) are the complex refractive indices (thickness) of air, NL-MX₂, SiO₂ and Si layers, respectively.

Similar to previous works^[1–4,8], to calculate the intensity of Raman signal from the multilayer structures, one must treat the laser excitation and Raman scattering processes separately. Raman signals from the depth z_3 in the Si layer will be excited by the laser excitation power at the corresponding depth. The multiple reflection and optical interference are also taken into account in the transition process of Raman signal from Si layer to air. We defined F_L and F_R as respective enhancement factors for laser excitation and Raman signal, similar to the notation of Yoon *et al.*^[2,4,8]. The Raman intensity of Si mode can be expressed by integrating over its thickness, d_{Si} , as the following equation:

$$I \propto \int_0^{d_{Si}} |F_L(z_3)F_R(z_3)|^2 dz_3. \quad (1)$$

The transfer matrix formalism can be used to calculate F_L and F_R in the multilayer structures, which has been widely used to calculate the Raman signal and optical contrast of NL flakes on SiO₂/Si substrate.^[3,5,6,8] Because the penetration depth of laser excitation into Si layer is far less than the actual thickness of Si substrate (d_3), the value of d_{Si} is taken as the penetration depth of laser excitation into Si layer in the numerical integration. In order to take the numerical aperture (N.A.) of the objective into account, we calculate contributions from each portion of the laser beam by integrating the incident angle θ from 0 to $\arcsin(N.A.)$. The s-polarization (transverse electric field, \vec{E} , perpendicular to the c-axis) and p-polarization (transverse magnetic field, \vec{H} , associated with the electric field by

$\vec{H} = \tilde{n}\vec{E}$) field components^[5] are also treated for the transfer matrices. Thus, the total Raman intensity of the Si mode is given by integrating over the solid angles (θ, φ for the laser beam and θ', φ' for the Raman signal) of the microscope objective and the depth z_3 in the Si layer:

$$I \propto \int_0^{d_{Si}} \int_0^{\arcsin(N.A.)} \int_0^{2\pi} \int_0^{\arcsin(N.A.)} \int_0^{2\pi} \sum_{i=s, p_{\perp}, p_{\parallel}} \sum_{j=s', p'_{\perp}, p'_{\parallel}} \left| F_L^i(z_3, \theta, \varphi) F_R^j(z_3, \theta', \varphi') \right|^2 \sin \theta \cos \theta d\theta d\varphi \sin \theta' \cos \theta' d\theta' d\varphi' dz_3, \quad (2)$$

We use the transfer matrix formalism calculate F_L and F_R in Eq. (2). The transmission and reflection of total electric and magnetic fields in the four-layer structure can be described by characteristic matrices A_{ij} and $B(z_j)$, where A_{ij} describes the propagation across the interface from i to j layer applying the boundary conditions, and $B(z_j)$ denotes the propagation through the j layer at depth z_j .

The s-polarization and p-polarization field components are treated separately in analyzing the characteristic matrices. $A_{ij}^{s(p)}$ can be expressed as follows:

$$A_{ij}^{s(p)} = \frac{1}{t_{ij}^{s(p)}} \begin{pmatrix} 1 & r_{ij}^{s(p)} \\ r_{ij}^{s(p)} & 1 \end{pmatrix} \quad (3)$$

where $t_{ij}^{s(p)}$ and $r_{ij}^{s(p)}$ are transmission and reflection coefficients from i to j layer for s-polarization and p-polarization, which depend on the complex refractive index \tilde{n}_i, \tilde{n}_j and the refractive angle θ_i, θ_j . The complex refractive index in the dielectric layer i is denoted by $\tilde{n}_i(\lambda) = n_i(\lambda) - \mathbf{i}k_i(\lambda)$, which is dependent on λ . Similar to previous works,^[8] we consider only the in-plane complex refractive index of NL-MX₂ flakes, and thus the s- and p-components of laser excitation can share the same expression. The refracted angle θ_i in the dielectric layer i is calculated with the Snell law as follows:

$$t_{ij}^s = \frac{2\tilde{n}_i \cos \theta_i}{\tilde{n}_i \cos \theta_i + \tilde{n}_j \cos \theta_j}, r_{ij}^s = \frac{\tilde{n}_i \cos \theta_i - \tilde{n}_j \cos \theta_j}{\tilde{n}_i \cos \theta_i + \tilde{n}_j \cos \theta_j}, t_{ij}^p = \frac{2\tilde{n}_i \cos \theta_i}{\tilde{n}_j \cos \theta_i + \tilde{n}_i \cos \theta_j}, r_{ij}^p = \frac{\tilde{n}_j \cos \theta_i - \tilde{n}_i \cos \theta_j}{\tilde{n}_j \cos \theta_i + \tilde{n}_i \cos \theta_j}.$$

$B(z_j)$ can be expressed as follows:

$$B(z_j) = \begin{pmatrix} e^{i\delta(z_j)} & 0 \\ 0 & e^{-i\delta(z_j)} \end{pmatrix} \quad (4)$$

where $\delta(z_j) = 2\pi\tilde{n}_j z_j \cos \theta_j / \lambda$ is phase factor, which is determined by the propagation distance z_j of laser or Raman scattering lights in j layer. The differences between the wavelengths of the laser and Si Raman peak should be considered in $t_{ij}^{s(p)}, r_{ij}^{s(p)}$ and $\delta(z_j)$ due to the λ -dependent complex refractive index for each layer. Finally, the complete transfer matrix for the whole multilayer structures can be obtained by multiplication of above simple matrices.

In the calculation of $I_{2D}(\text{Si})$, the laser approaches at the Si layer and is absorbed finally, and thus there is no laser components transmitting toward the surface at any depths in the Si layer, as illustrated in Fig. S1. The transfer equation for the laser beam transmitting from air to the depth z_3 in the Si layer is expressed as follows:

$$\begin{pmatrix} E_{L0}^{s(p),+} \\ E_{L0}^{s(p),-} \end{pmatrix} = A_{01}^{s(p)} B(d_1) A_{12}^{s(p)} B(d_2) A_{23}^{s(p)} B(z_3) \begin{pmatrix} E_{LS}^{s(p),+}(z_3) \\ 0 \end{pmatrix} \quad (5)$$

where the symbols $+$, $-$ denote light propagating directions from air to the dielectric layers and the opposite direction. $E_{L0}^{s(p),+}$ is the electric field component of laser source in air, which is assumed as 1. $E_{LS}^{s(p),+}(z_3)$ is the electric field component at the depth z_3 in Si layer. The laser excitation enhancement factors in this process can be calculated by $F_L^s(z_3) = E_{LS}^{s,+}(z_3)$, $F_L^{p\perp}(z_3) = E_{LS}^{p,+}(z_3) \cos \theta_3$ and $F_L^{p\parallel}(z_3) = E_{LS}^{p,+}(z_3) \sin \theta_3$. $E_{LS}^{s(p),+}(z_3)$ can be calculated with the transfer equation Eq. (5) and $F_L^{s(p\perp,p\parallel)}(z_3)$ can be obtained.

For the Raman scattering process of the Si mode, only one pathway for the emission of Raman signal toward (up,U) the NL-MX₂ surface is considered, and that away from (down,D) the NL-MX₂ surface is absorbed by the Si layer, as illustrated in Fig. S1. The transfer equation for the Raman signal excited by the laser at the depth z_3 in the Si layer is expressed as follows:

$$\begin{pmatrix} 0 \\ E_{RU0}^{s'(p'),-} \end{pmatrix} = A_{01}^{s'(p')} B(d_1) A_{12}^{s'(p')} B(d_2) A_{23}^{s'(p')} B(z_3) \begin{pmatrix} E_{RUS}^{s'(p'),+}(z_3) \\ E_{RUS}^{s'(p'),-}(z_3) \end{pmatrix} \quad (6)$$

where $E_{RU0}^{s'(p'),-}(z_3)$ is the electric field component of Raman signal source related with 'U' pathway at the depth z_3 in the Si layer and is assumed as 1.

The Raman scattering enhancement factors in this process can be calculated by $F_R^{s'}(z_3) = E_{RU0}^{s',-}$, $F_R^{p'\perp}(z_3) = E_{RU0}^{p',-} \cos \theta'_3$ and $F_R^{p'\parallel}(z_3) = E_{RU0}^{p',-} \sin \theta'_3$. $E_{RU0}^{s'(p'),-}$ can be calculated by the transfer equation Eq. (6) and $F_R^{s'(p'\perp,p'\parallel)}(z_3)$ can be obtained.

The total Raman intensity of $I_{2D}(\text{Si})$ from SiO₂/Si substrates underneath TMD flakes can be calculated by the formula of Eq. (2).

$I_0(\text{Si})$ from bare SiO₂/Si substrates can be calculated directly based on the above model once the thickness of NL flakes is set to zero.

2. $I_{2D}(\text{Si})/I_0(\text{Si})$ for NL-TMDs deposited on SiO_2/Si substrate

As demonstrated in the main text, the calculated $I_{2D}(\text{Si})/I_0(\text{Si})$ of NL-TMDs based on the \tilde{n}_{eff} for different ϵ_L can be used for N determination of NL-TMDs flakes deposited on SiO_2/Si substrates. $I_{2D}(\text{Si})/I_0(\text{Si})$ is expected to be sensitive to N, N.A., ϵ_L and h_{SiO_2} .^[8] It is evident that a variation of 10 nm for h_{SiO_2} can introduce a change on the N-dependent $I_{2D}(\text{Si})/I_0(\text{Si})$, therefore, a precise determination of h_{SiO_2} is very important for N identification of NL-TMDs flakes on SiO_2/Si substrates by $I_{2D}(\text{Si})/I_0(\text{Si})$.

It is found that an effective N.A. must be used for optical contrast calculation of multilayer graphene deposited on SiO_2/Si substrates once the $100\times$ objective with N.A. of ~ 0.9 is used for optical microscope.^[5,6] If one uses an objective with N.A. less than 0.5 for the measurement of optical contrast, the actual N.A. can be used for the theoretical calculation of optical contrast for N identification of two-dimensional flakes.^[6] For the sake of N identification of TMD flakes for research community, $I_{2D}(\text{Si})/I_0(\text{Si})$ of NL-MoS₂, NL-WS₂ and NL-WeS₂ excited by commonly-used 2.54-eV and 2.34-eV excitations for $80\text{nm} < h_{\text{SiO}_2} < 110\text{nm}$ and $280\text{nm} < h_{\text{SiO}_2} < 310\text{nm}$ are calculated and here the objective N.A. of 0.35 (Olympus SLMPLN $50\times$ objective with a long-working distance of 18mm) and of 0.50 (Olympus LMPLFLN $50\times$ objective with a long-working distance of 10.6mm) is considered in the calculation. The results are summarized in Table 1-6. We find that $I_{2D}(\text{Si})/I_0(\text{Si})$ is not sensitive to N.A. when $\text{N.A.} \leq 0.5$ and $N \leq 10$.

For an approximation, $I_{2D}(\text{Si})/I_0(\text{Si})$ for any h_{SiO_2} in the range of 80-110nm or 280-310nm can be obtained by the interpolation between the two values corresponding to two nearest h_{SiO_2} .

3. $I_{2D}(\text{Si})/I_0(\text{Si})$ for N Layer graphenes deposited on SiO_2/Si substrate

$I_{2D}(\text{Si})/I_0(\text{Si})$ has been used to identify N of intrinsic and defective multilayer graphenes up to $N = 100$.^[8] For a purpose of practise application, the calculation values of $I_{2D}(\text{Si})/I_0(\text{Si})$ are provided here for several typical h_{SiO_2} (80-110nm or 280-310nm), commonly-used ϵ_L (2.34 and 1.96 eV) and the objective N.A. (0.35 and 0.50), as summarized in Table 7 and Table 8. $I_{2D}(\text{Si})/I_0(\text{Si})$ is not sensitive to N.A. when $\text{N.A.} \leq 0.5$ and $N \leq 15$ for NL graphenes deposited on SiO_2/Si substrate.

For an approximation, $I_{2D}(\text{Si})/I_0(\text{Si})$ for any h_{SiO_2} in the range of 80-110nm or 280-310nm can be

obtained by the interpolation between the two values corresponding to two nearest h_{SiO_2} .

References

- [1] Y. Y. Wang, Z. H. Ni, Z. X. Shen, H. M. Wang and Y. H. Wu, Appl. Phys. Lett., 2008, 92, 043121.
- [2] D. Yoon, H. Moon, Y.-W. Son, J. S. Choi, B. H. Park, Y. H. Cha, Y. D. Kim and H. Cheong, Phys. Rev. B, 2009, 80, 125422.
- [3] Y. K. Koh, M.-H. Bae, D. G. Cahill, E. Pop, ACS Nano, 2011, 5, 269.
- [4] S.-L. Li, H. Miyazaki, H. Song, H. Kuramochi, S. Nakaharai and K. Tsukagoshi, ACS Nano, 2012, 6, 7381.
- [5] C. Casiraghi, A. Hartschuh, E. Lidorikis, H. Qian, H. Harutyunyan, T. Gokus, K. S. Novoselov, A. C. Ferrari, Nano Letters, 2007, 7, 2711.
- [6] W. P. Han, Y. M. Shi, X. L. Li, S. Q. Luo, Y. Lu and P. H. Tan, Acta Phys. Sin., 2013, 62, 110702.
- [7] V. G. Kravets, A. N. Grigorenko, R. R. Nair, P. Blake, S. Anissimova, K. S. Novoselov, A. K. Geim, Phys. Rev. B, 2010, 81, 155413.
- [8] X. L. Li, X. F. Qiao, W. P. Han, Y. Lu, Q. H. Tan, X. L. Liu, P. H. Tan, Nanoscale, 2015, 7, 8135.

Table 1 $I_{2D}(\text{Si})/I_0(\text{Si})$ of NL-MoS₂ flakes deposited on SiO₂/Si substrate as a function of N for h_{SiO_2} =80nm, 90nm, 100nm, 110nm, and 280nm, 290nm, 300nm, 310nm. ϵ_L =2.54 eV and N.A.=0.35 and 0.50. \tilde{n} of NL-MoS₂, SiO₂ and Si are 5.29-1.85*i*, 1.462, 4.360-0.086*i*.

h_{SiO_2}	80nm		90nm		100nm		110nm		280nm		290nm		300nm		310nm	
NA	0.35	0.5	0.35	0.5	0.35	0.5	0.35	0.5	0.35	0.5	0.35	0.5	0.35	0.5	0.35	0.5
1L	0.686	0.693	0.644	0.649	0.624	0.626	0.627	0.625	0.627	0.627	0.645	0.636	0.679	0.661	0.723	0.699
2L	0.466	0.474	0.420	0.425	0.402	0.404	0.409	0.407	0.408	0.407	0.433	0.421	0.477	0.454	0.537	0.505
3L	0.318	0.325	0.281	0.285	0.268	0.269	0.277	0.275	0.276	0.273	0.301	0.289	0.346	0.323	0.409	0.375
4L	0.220	0.226	0.192	0.195	0.185	0.185	0.194	0.192	0.193	0.190	0.216	0.205	0.257	0.236	0.318	0.285
5L	0.156	0.160	0.135	0.137	0.131	0.131	0.140	0.138	0.139	0.135	0.160	0.149	0.196	0.177	0.252	0.222
6L	0.112	0.116	0.097	0.099	0.095	0.095	0.104	0.102	0.103	0.099	0.121	0.112	0.153	0.136	0.203	0.175
7L	0.083	0.085	0.072	0.073	0.071	0.071	0.079	0.077	0.078	0.075	0.093	0.085	0.121	0.106	0.166	0.141
8L	0.062	0.064	0.054	0.055	0.054	0.054	0.061	0.060	0.060	0.057	0.073	0.067	0.098	0.085	0.137	0.116
9L	0.048	0.049	0.042	0.043	0.042	0.042	0.048	0.047	0.047	0.045	0.059	0.053	0.080	0.069	0.115	0.096
10L	0.037	0.038	0.033	0.033	0.033	0.033	0.039	0.038	0.038	0.036	0.048	0.043	0.066	0.057	0.098	0.081

Table 2 $I_{2D}(\text{Si})/I_0(\text{Si})$ of NL-MoS₂ flakes deposited on SiO₂/Si substrate as a function of N for h_{SiO_2} =80nm, 90nm, 100nm, 110nm, and 280nm, 290nm, 300nm, 310nm. ϵ_L =2.34 eV and N.A.=0.35 and 0.50. \tilde{n} of NL-MoS₂, SiO₂ and Si are 4.85-1.20*i*, 1.460, 4.143-0.054*i*.

h_{SiO_2}	80nm		90nm		100nm		110nm		280nm		290nm		300nm		310nm	
NA	0.35	0.5	0.35	0.5	0.35	0.5	0.35	0.5	0.35	0.5	0.35	0.5	0.35	0.5	0.35	0.5
1L	0.855	0.862	0.806	0.813	0.770	0.775	0.748	0.751	0.796	0.817	0.764	0.779	0.746	0.755	0.745	0.746
2L	0.708	0.719	0.637	0.646	0.587	0.593	0.561	0.564	0.622	0.652	0.580	0.600	0.560	0.570	0.561	0.560
3L	0.574	0.587	0.497	0.507	0.447	0.453	0.423	0.426	0.482	0.514	0.440	0.461	0.423	0.432	0.428	0.426
4L	0.459	0.472	0.386	0.395	0.342	0.348	0.323	0.325	0.373	0.403	0.337	0.354	0.324	0.330	0.331	0.327
5L	0.365	0.377	0.300	0.308	0.263	0.268	0.249	0.251	0.290	0.315	0.260	0.274	0.250	0.255	0.259	0.255
6L	0.290	0.300	0.235	0.241	0.205	0.209	0.194	0.196	0.226	0.248	0.202	0.214	0.196	0.200	0.206	0.201
7L	0.230	0.239	0.185	0.190	0.161	0.164	0.154	0.155	0.178	0.196	0.159	0.168	0.156	0.158	0.165	0.161
8L	0.184	0.191	0.147	0.151	0.128	0.130	0.123	0.124	0.141	0.156	0.127	0.134	0.125	0.126	0.134	0.130
9L	0.148	0.154	0.117	0.121	0.103	0.105	0.100	0.100	0.113	0.125	0.102	0.108	0.102	0.102	0.111	0.106
10L	0.120	0.125	0.095	0.098	0.083	0.085	0.082	0.082	0.092	0.101	0.083	0.088	0.083	0.084	0.092	0.088

Table 3 $I_{2D}(\text{Si})/I_0(\text{Si})$ of NL-WS₂ flakes deposited on SiO₂/Si substrate as a function of N for h_{SiO_2} =80nm, 90nm, 100nm, 110nm, and 280nm, 290nm, 300nm, 310nm. ϵ_L =2.54 eV and N.A.=0.35 and 0.50. \tilde{n} of NL-WS₂, SiO₂ and Si are 4.40-1.10*i*, 1.462, 4.360-0.086*i*.

h_{SiO_2}	80nm		90nm		100nm		110nm		280nm		290nm		300nm		310nm	
NA	0.35	0.5	0.35	0.5	0.35	0.5	0.35	0.5	0.35	0.5	0.35	0.5	0.35	0.5	0.35	0.5
1L	0.833	0.839	0.791	0.796	0.766	0.769	0.760	0.760	0.762	0.766	0.769	0.765	0.790	0.779	0.820	0.804
2L	0.679	0.689	0.620	0.627	0.589	0.592	0.583	0.583	0.585	0.589	0.598	0.591	0.631	0.614	0.680	0.654
3L	0.547	0.558	0.485	0.492	0.455	0.458	0.453	0.452	0.453	0.456	0.471	0.462	0.511	0.490	0.569	0.538
4L	0.438	0.448	0.380	0.386	0.354	0.357	0.355	0.354	0.355	0.357	0.376	0.366	0.418	0.396	0.480	0.447
5L	0.349	0.359	0.299	0.305	0.278	0.280	0.282	0.280	0.282	0.282	0.303	0.293	0.345	0.324	0.409	0.375
6L	0.279	0.288	0.237	0.242	0.221	0.223	0.227	0.225	0.226	0.225	0.247	0.237	0.288	0.267	0.351	0.318
7L	0.224	0.232	0.189	0.194	0.178	0.179	0.184	0.182	0.183	0.182	0.204	0.194	0.243	0.223	0.304	0.271
8L	0.181	0.188	0.153	0.156	0.144	0.145	0.151	0.149	0.150	0.148	0.170	0.160	0.207	0.188	0.265	0.234
9L	0.148	0.153	0.124	0.127	0.118	0.119	0.125	0.124	0.124	0.122	0.143	0.134	0.178	0.160	0.233	0.203
10L	0.121	0.125	0.102	0.104	0.098	0.098	0.105	0.104	0.104	0.102	0.122	0.113	0.154	0.137	0.206	0.178

Table 4 $I_{2D}(\text{Si})/I_0(\text{Si})$ of NL-WS₂ flakes deposited on SiO₂/Si substrate as a function of N for h_{SiO_2} =80nm, 90nm, 100nm, 110nm, and 280nm, 290nm, 300nm, 310nm. ϵ_L =2.34 eV and N.A.=0.35 and 0.50. \tilde{n} of NL-WS₂, SiO₂ and Si are 4.62-0.48*i*, 1.460, 4.143-0.054*i*.

h_{SiO_2}	80nm		90nm		100nm		110nm		280nm		290nm		300nm		310nm	
NA	0.35	0.5	0.35	0.5	0.35	0.5	0.35	0.5	0.35	0.5	0.35	0.5	0.35	0.5	0.35	0.5
1L	0.970	0.977	0.920	0.927	0.875	0.882	0.844	0.848	0.907	0.930	0.866	0.886	0.839	0.853	0.826	0.833
2L	0.908	0.922	0.819	0.831	0.747	0.757	0.701	0.707	0.798	0.837	0.734	0.765	0.695	0.715	0.679	0.688
3L	0.824	0.842	0.710	0.725	0.626	0.638	0.576	0.583	0.686	0.734	0.612	0.647	0.571	0.592	0.557	0.565
4L	0.728	0.748	0.603	0.619	0.519	0.530	0.471	0.478	0.578	0.629	0.505	0.540	0.467	0.487	0.458	0.463
5L	0.629	0.650	0.505	0.521	0.426	0.437	0.385	0.391	0.482	0.532	0.415	0.447	0.382	0.399	0.377	0.380
6L	0.535	0.555	0.419	0.433	0.349	0.359	0.315	0.320	0.399	0.444	0.340	0.368	0.313	0.327	0.312	0.313
7L	0.450	0.468	0.346	0.359	0.286	0.294	0.259	0.263	0.328	0.369	0.279	0.303	0.258	0.269	0.259	0.259
8L	0.376	0.392	0.285	0.296	0.235	0.242	0.213	0.217	0.271	0.306	0.229	0.249	0.214	0.222	0.217	0.216
9L	0.313	0.327	0.235	0.245	0.194	0.200	0.177	0.180	0.223	0.253	0.190	0.206	0.178	0.184	0.183	0.181
10L	0.260	0.273	0.195	0.203	0.161	0.166	0.148	0.150	0.185	0.210	0.158	0.171	0.149	0.154	0.155	0.153

Table 5 $I_{2D}(\text{Si})/I_0(\text{Si})$ of NL-WeS₂ flakes deposited on SiO₂/Si substrate as a function of N for h_{SiO_2} =80nm, 90nm, 100nm, 110nm, and 280nm, 290nm, 300nm, 310nm. ϵ_L =2.54 eV and N.A.=0.35 and 0.50. \tilde{n} of NL-WeS₂, SiO₂ and Si are 4.22-1.86*i*, 1.462, 4.360-0.086*i*.

h_{SiO_2}	80nm		90nm		100nm		110nm		280nm		290nm		300nm		310nm	
NA	0.35	0.5	0.35	0.5	0.35	0.5	0.35	0.5	0.35	0.5	0.35	0.5	0.35	0.5	0.35	0.5
1L	0.728	0.733	0.700	0.703	0.690	0.690	0.698	0.695	0.697	0.694	0.717	0.707	0.748	0.732	0.786	0.766
2L	0.533	0.539	0.498	0.502	0.489	0.489	0.501	0.498	0.499	0.495	0.528	0.513	0.572	0.549	0.628	0.598
3L	0.394	0.400	0.362	0.365	0.354	0.355	0.369	0.365	0.367	0.362	0.398	0.382	0.446	0.421	0.510	0.476
4L	0.295	0.300	0.268	0.271	0.263	0.263	0.278	0.275	0.276	0.270	0.306	0.291	0.354	0.329	0.419	0.384
5L	0.223	0.228	0.202	0.204	0.199	0.199	0.214	0.210	0.211	0.206	0.240	0.226	0.285	0.262	0.349	0.315
6L	0.172	0.176	0.155	0.157	0.154	0.153	0.167	0.164	0.165	0.160	0.191	0.178	0.233	0.211	0.294	0.261
7L	0.134	0.137	0.120	0.122	0.121	0.120	0.133	0.130	0.131	0.126	0.154	0.143	0.193	0.173	0.250	0.219
8L	0.106	0.109	0.095	0.096	0.096	0.096	0.107	0.105	0.105	0.101	0.126	0.116	0.162	0.143	0.215	0.186
9L	0.085	0.087	0.076	0.077	0.078	0.077	0.088	0.086	0.086	0.082	0.105	0.096	0.137	0.120	0.186	0.159
10L	0.068	0.070	0.062	0.063	0.063	0.063	0.073	0.071	0.071	0.068	0.088	0.080	0.117	0.102	0.162	0.138

Table 6 $I_{2D}(\text{Si})/I_0(\text{Si})$ of NL-WeS₂ flakes deposited on SiO₂/Si substrate as a function of N for h_{SiO_2} =80nm, 90nm, 100nm, 110nm, and 280nm, 290nm, 300nm, 310nm. ϵ_L =2.34 eV and N.A.=0.35 and 0.50. \tilde{n} of NL-WeS₂, SiO₂ and Si are 4.64-1.40i, 1.460, 4.143-0.054i.

h_{SiO_2}	80nm		90nm		100nm		110nm		280nm		290nm		300nm		310nm	
NA	0.35	0.5	0.35	0.5	0.35	0.5	0.35	0.5	0.35	0.5	0.35	0.5	0.35	0.5	0.35	0.5
1L	0.822	0.829	0.778	0.784	0.746	0.750	0.729	0.730	0.769	0.788	0.741	0.754	0.728	0.735	0.731	0.729
2L	0.660	0.670	0.598	0.606	0.556	0.561	0.536	0.538	0.586	0.612	0.550	0.567	0.537	0.544	0.543	0.540
3L	0.523	0.534	0.457	0.466	0.417	0.422	0.400	0.401	0.446	0.472	0.412	0.428	0.401	0.407	0.410	0.406
4L	0.412	0.422	0.351	0.358	0.315	0.320	0.302	0.304	0.341	0.365	0.312	0.326	0.304	0.308	0.315	0.310
5L	0.323	0.333	0.270	0.277	0.241	0.245	0.232	0.233	0.262	0.283	0.239	0.250	0.234	0.237	0.246	0.240
6L	0.255	0.263	0.210	0.216	0.187	0.190	0.181	0.181	0.204	0.221	0.185	0.194	0.183	0.185	0.195	0.189
7L	0.202	0.209	0.165	0.170	0.147	0.149	0.143	0.143	0.160	0.174	0.146	0.153	0.145	0.146	0.156	0.151
8L	0.161	0.167	0.131	0.135	0.116	0.118	0.114	0.114	0.127	0.139	0.116	0.122	0.116	0.117	0.127	0.122
9L	0.129	0.134	0.105	0.108	0.094	0.095	0.092	0.092	0.102	0.111	0.093	0.098	0.095	0.094	0.105	0.100
10L	0.105	0.109	0.085	0.088	0.076	0.077	0.076	0.076	0.082	0.090	0.076	0.080	0.078	0.077	0.087	0.082

Table 7 $I_{2D}(\text{Si})/I_0(\text{Si})$ of NLG flakes deposited on SiO_2/Si substrate as a function of N for h_{SiO_2} =80nm, 90nm, 100nm, 110nm, and 280nm, 290nm, 300nm, 310nm. ϵ_L =2.34 eV and N.A.=0.35 and 0.50. \tilde{n} of NLG, SiO_2 and Si are 2.725-1.366*i*, 1.460, 4.143-0.054*i*.

h_{SiO_2}	80nm		90nm		100nm		110nm		280nm		290nm		300nm		310nm	
NA	0.35	0.5	0.35	0.5	0.35	0.5	0.35	0.5	0.35	0.5	0.35	0.5	0.35	0.5	0.35	0.5
1L	0.938	0.939	0.929	0.930	0.924	0.924	0.923	0.923	0.927	0.931	0.924	0.926	0.924	0.924	0.928	0.926
2L	0.879	0.882	0.863	0.866	0.854	0.856	0.853	0.853	0.861	0.868	0.854	0.858	0.855	0.855	0.863	0.859
3L	0.824	0.828	0.803	0.806	0.791	0.793	0.790	0.790	0.800	0.809	0.791	0.796	0.792	0.792	0.803	0.798
4L	0.773	0.778	0.748	0.751	0.733	0.735	0.732	0.732	0.744	0.755	0.733	0.739	0.735	0.735	0.749	0.742
5L	0.726	0.731	0.696	0.701	0.681	0.683	0.680	0.679	0.692	0.704	0.680	0.687	0.683	0.682	0.699	0.691
6L	0.681	0.687	0.649	0.654	0.632	0.635	0.632	0.631	0.644	0.658	0.632	0.639	0.636	0.635	0.653	0.645
7L	0.639	0.646	0.606	0.611	0.588	0.591	0.588	0.588	0.601	0.615	0.588	0.595	0.592	0.591	0.611	0.602
8L	0.600	0.607	0.565	0.571	0.548	0.551	0.548	0.548	0.561	0.575	0.548	0.555	0.553	0.551	0.573	0.563
9L	0.564	0.571	0.528	0.534	0.511	0.513	0.511	0.511	0.523	0.539	0.511	0.518	0.516	0.515	0.538	0.527
10L	0.530	0.538	0.494	0.500	0.477	0.479	0.478	0.477	0.489	0.504	0.477	0.484	0.483	0.481	0.505	0.494
11L	0.499	0.506	0.463	0.468	0.445	0.448	0.447	0.446	0.458	0.473	0.446	0.453	0.452	0.450	0.475	0.464
12L	0.469	0.477	0.433	0.439	0.417	0.419	0.418	0.418	0.429	0.444	0.417	0.424	0.424	0.422	0.447	0.436
13L	0.442	0.449	0.406	0.412	0.390	0.393	0.392	0.392	0.402	0.417	0.391	0.397	0.398	0.395	0.421	0.410
14L	0.416	0.423	0.381	0.386	0.366	0.368	0.368	0.368	0.377	0.391	0.367	0.373	0.374	0.371	0.398	0.386
15L	0.392	0.399	0.358	0.363	0.343	0.345	0.346	0.346	0.354	0.368	0.344	0.350	0.352	0.349	0.376	0.364

Table 8 $I_{2D}(\text{Si})/I_0(\text{Si})$ of NLG flakes deposited on SiO_2/Si substrate as a function of N for h_{SiO_2} =80nm, 90nm, 100nm, 110nm, and 280nm, 290nm, 300nm, 310nm. ϵ_L =1.96 eV and N.A.=0.35 and 0.50. \tilde{n} of NLG, SiO_2 and Si are 2.819-1.450i, 1.457, 3.879-0.021i.

h_{SiO_2}	80nm		90nm		100nm		110nm		280nm		290nm		300nm		310nm	
NA	0.35	0.5	0.35	0.5	0.35	0.5	0.35	0.5	0.35	0.5	0.35	0.5	0.35	0.5	0.35	0.5
1L	0.955	0.957	0.948	0.949	0.940	0.942	0.935	0.936	0.972	0.975	0.966	0.969	0.959	0.963	0.951	0.955
2L	0.913	0.915	0.898	0.900	0.885	0.887	0.874	0.876	0.945	0.950	0.933	0.939	0.919	0.926	0.904	0.912
3L	0.872	0.875	0.851	0.854	0.832	0.836	0.818	0.821	0.918	0.925	0.901	0.910	0.881	0.891	0.860	0.871
4L	0.832	0.836	0.806	0.811	0.783	0.788	0.766	0.770	0.892	0.901	0.869	0.881	0.844	0.857	0.818	0.832
5L	0.794	0.799	0.764	0.769	0.738	0.742	0.718	0.722	0.866	0.877	0.838	0.852	0.808	0.824	0.777	0.794
6L	0.758	0.764	0.724	0.730	0.695	0.700	0.674	0.678	0.840	0.853	0.808	0.824	0.773	0.792	0.739	0.758
7L	0.723	0.730	0.686	0.692	0.655	0.661	0.632	0.637	0.815	0.830	0.779	0.797	0.740	0.761	0.702	0.723
8L	0.690	0.697	0.650	0.657	0.617	0.623	0.594	0.598	0.790	0.807	0.751	0.771	0.709	0.731	0.668	0.690
9L	0.658	0.666	0.617	0.624	0.582	0.589	0.558	0.563	0.766	0.784	0.723	0.745	0.678	0.702	0.635	0.658
10L	0.628	0.636	0.585	0.592	0.550	0.556	0.525	0.530	0.743	0.762	0.697	0.720	0.649	0.674	0.604	0.628
11L	0.599	0.607	0.555	0.562	0.519	0.525	0.494	0.499	0.720	0.740	0.671	0.696	0.621	0.647	0.574	0.600
12L	0.572	0.580	0.526	0.534	0.490	0.497	0.466	0.470	0.697	0.719	0.646	0.672	0.594	0.621	0.546	0.572
13L	0.546	0.554	0.500	0.507	0.463	0.470	0.439	0.444	0.675	0.698	0.622	0.649	0.569	0.596	0.520	0.546
14L	0.521	0.529	0.474	0.482	0.438	0.445	0.414	0.419	0.654	0.678	0.599	0.626	0.544	0.573	0.495	0.521
15L	0.497	0.506	0.450	0.458	0.414	0.421	0.391	0.395	0.633	0.658	0.576	0.605	0.521	0.550	0.471	0.498